Inherent Irreversibility of Mixed Convection within Concentric Pipes in a Porous Medium with Thermal Radiation

Oluwole Daniel Makinde[1], Adetayo Samuel Eegunjobi[2*]

[1]Faculty of Military Science, Stellenbosch University, Private Bag X2, Saldanha 7395, South Africa
[2]Mathematics Department, Namibia University of Science and Technology, Windhoek 9000, Namibia
[*]E-mail: samdet1@yahoo.com

Abstract. This work investigated the thermal putrefaction and inherent irreversibility in a steady flow of an incompressible inconstant viscosity radiating fluid within two concentric pipes filled with a porous medium. Following the Brinkmann-Darcy-Forchheimer approach, the nonlinear differential equations governing the model were obtained. The model boundary value problem was addressed numerically via a shooting quadrature with the Runge-Kutta-Fehlberg integration scheme. The effects of diverse emerging parameters on the fluid velocity, temperature, skin friction, Nusselt number, entropy generation rate and the Bejan number are provided in graphs and discussed in this paper.

Keywords: *buoyancy force; concentric pipes; entropy analysis; porous medium; thermal radiation; variable viscosity fluid.*

1 Introduction

In recent years convective flow in a concentric annulus has attracted much attention owing to its importance for industrial and engineering applications such as aero-engines, thermal energy storage systems, cooling of electronic components and transmission cables, oil and gas drilling wells, and extruders, just to mention a few. In all these applications, the two concentric cylinders may be fixed, moving, or one fixed and the other moving during operation. Watanabe *et al.* [1] carried out a theoretical and experimental study on the fluid flows inside two concentric cylinders coupled with vertical axes. They surmised that the inner cylinder movement changes the flow structure. They also reported that the critical Reynolds numbers fluctuate at the free surface as the kinetic energy in the velocity component surges precipitously. Fénot *et al.* [2] surveyed the heat transfer of the flow between concentrically spinning cylinders and compared the different gap thickness, axial radial ratio, and velocity rotational of some works. Makinde [3] numerically examined the problem of steady universal axial Couette flow of Ostwald-de Waele power-law responsive fluids

Received February 15th, 2021, Revised August 27th, 2021, Accepted for publication November 18th, 2021
 ISSN: 2337-5760,
DOI: 10.5614/j.math.fund.sci.2021.53.3.5

between two concentric cylindrical tubes. The fixed outside cylinder trades heat with the surrounding conditions following Newton's law of cooling while the isothermal inside cylinder moved in an axial direction. The work revealed the thermal criticality for the onset of instability in the flow environment. It was reported that the entire circulating structure and thermal decomposition strongly depend on the embedded thermophysical parameters. The heat transfer capability of a viscoelastic fluid in an annular flow within two rotating concentric cylinders was analytically examined by Lorenzini *et al.* [4] using the Giesekus model. It was found that a rise in Brinkmann number may lead to asymptotic behavior of the Nusselt number. Coelho *et al.* [5] theoretically examined the impact of an embedded porous medium in conduit flows of a non-Newtonian fluid and obtained a generalized Brinkmann number that is valid for any flow regime to calculate the proportion of frictional heat and heat exchange at the wall.

The thermodynamic performance of engineering systems can be enhanced by effectively regulating various factors related to entropy generation. Thermodynamic irreversibility and entropy generation are connected, and this happens in practically all flow and heat exchange activities. Bejan [6] presents an investigation of the second law of fluid flow and heat transfer with entropy minimization in a thermal device. He obtained a suitable analytical solution (entropy generation number) to estimate the destruction of available work in a flow process involving heat transfer.

Thereafter, several authors [7-10] have investigated entropy generation minimization in fluid currents with heat and mass exchange problems under various physical conditions. Yurusoy *et al.* [11] investigated the problem of heat exchange characteristics in a non-Newtonian fluid flow inside annulated pipes with entropy generation. Their study revealed that a reduction of the non-Newtonian parameter increases the inherent irreversibility in the flow regime. The combined influence of thermal radiation, buoyancy force, convective cooling and viscous dissipation on entropy generation rate in the microchannel flow of an EG/Ag nanofluid was numerically studied by Monaledi & Makinde [12]. They found that an increase in nanoparticle volume fraction, buoyancy forces and thermal radiation boosts the thermodynamic irreversibility in the flow regime.

Chakraborty & Ray [13] made use of the laws of thermodynamics, both the first and second, to investigate entropy generation minimization criteria in a thermal-hydraulic duct flow with round corners. It was shown that the geometry of the ducts may not greatly influence the thermodynamic irreversibility in the flow regime. The inherent irreversibility in an unsteady Poiseuille-Rayleigh-Bénard hydromagnetic blended convection through a channel was numerically

investigated by Marzougui *et al.* [14]. Their results revealed that a variation in Brinkmann number considerably affected the entropy generation rate within the flow regime. Recently, Mebarek-Oudina *et al.* [15] numerically investigated the consequences of a magnetic field on the thermodynamic irreversibility inside an enclosed trapezoidal cavity with a zig-zag wall containing a hybrid nano-liquid with heat transfer. They reported that an increase in magnetic field intensity reduces the entropy production rate. For interested readers, further relevant recent literature on entropy generation minimization in fluid flows with heat exchange features can be found in [16-18].

From a literature survey, it was found that the combined impacts of Brinkmann-Darcy-Forchheimer porous medium, thermal radiation, velocity slip, and variable viscosity on thermodynamic irreversibility in buoyant convection within a concentric annulus have not been thoroughly investigated yet. Hence, the present work aimed to fill this gap in the literature. Buoyant transmittal in an annular configuration filled with porous media consisting of two concentric pipes has many important applications, namely, in heat exchange systems in metallurgical and petrochemical procedures, moisture migration in fibrous insulation, underground discarding of nuclear wastes, and thermal converters with a porous liner. In the next section, the controlling equations of the problem are given; the equations are therefore dimensionless and solved numerically. The consequences of diverse rooted parameters on the velocity profile, temperature profile, skin friction, Nusselt number, entropy generation rate and the Bejan number are provided with graphs and discussed.

2 Model

We address an incompressible changeable viscosity fluid steady flow through the annulus inside two concentric vertical pipes loaded with a penetrable medium in addition to the united action of thermal buoyancy and axial pressure gradient. The inner pipe surface was assumed to be slippery and maintained at a uniform high temperature, T_0 (this assumption illustrates the occurrence of a heat-generating mechanical process within the hollow of the inner pipe), while the outer pipe surface was adapted to convective heat swap with the ambient environment following Newton's law of cooling, as pictured in Figure 1. To describe the flow of the fluid through a porous medium with high enough velocity, the Brinkmann-Darcy-Forchheimer model was employed. The Forchheimer model incorporates two terms that indicate the viscous effect and the inertial effect. The model utilizes the square root of permeability as the corresponding length characteristics are in agreement with the linearized Darcy law at low velocities, while the non-dimensional coefficient in the quadratic term is used to represent the inertial effect.

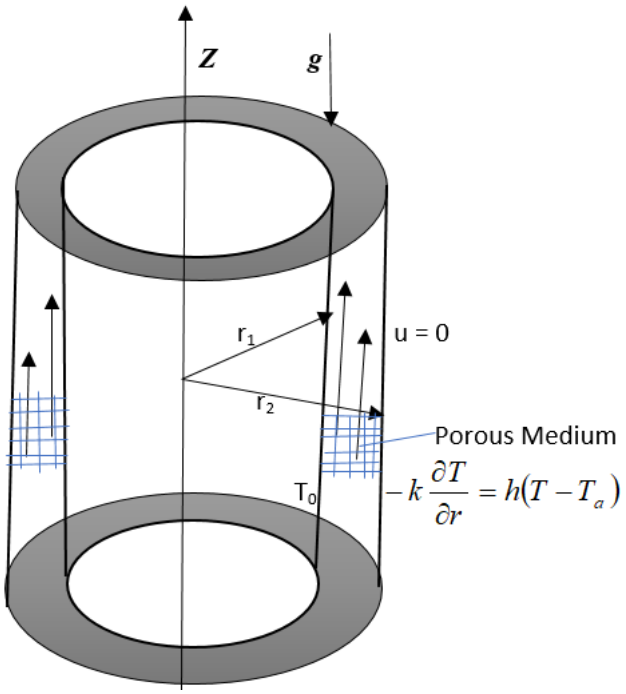

Figure 1 Schematic diagram of the model.

With these assumptions, the continuity, momentum, energy and volumetric entropy generation equations take the following form [3,4,7,11];

$$\frac{\partial u}{\partial z} = 0, \tag{1}$$

$$-\frac{\partial P}{\partial z} + \frac{1}{r}\frac{\partial}{\partial r}\left(r\mu(T)\frac{\partial u}{\partial r}\right) + g\beta(T - T_a) - \frac{\mu(T)u}{K} - \frac{\rho c u^2}{\sqrt{K}} = 0, \tag{2}$$

$$\frac{k}{r}\frac{\partial}{\partial r}\left(r\frac{\partial T}{\partial r}\right) - \frac{\partial q_r}{\partial r} + \mu(T)\left(\frac{\partial u}{\partial r}\right)^2 + \frac{\mu(T)u^2}{K} + \frac{cu^3}{\sqrt{K}} = 0, \tag{3}$$

$$E_G = \frac{k}{(T_0 - T_a)^2}\left(1 + \frac{16\sigma^* T_a^3}{3kk^*}\right)\left[\frac{\partial T}{\partial r}\right]^2 + \frac{\mu(T)}{(T_0 - T_a)}\left(\frac{\partial u}{\partial r}\right)^2 + \frac{\mu(T)u^2}{(T_0 - T_a)K} + \frac{cu^3}{(T_0 - T_a)\sqrt{K}}. \tag{4}$$

The relevant boundary conditions at both the inner slip surface and the outer convective cooling surface are as follows:

$$u = \frac{\mu(T_0)}{\delta}\frac{\partial u}{\partial r}, \quad T = T_0, \quad \text{at r} = r_1, \tag{5}$$

$$u = 0, \quad -k\frac{\partial T}{\partial r} = h(T - T_a), \quad \text{at r} = r_2. \tag{6}$$

In line with the Roseland approximation [19,20], the local radiative heat flux term for an optically thick gray fluid is given by

$$q_r = -\frac{4\sigma*}{3k*}\frac{\partial T^4}{\partial r} \approx -\frac{16\sigma*T_a^3}{3k*}\frac{\partial T}{\partial r}, \tag{7}$$

where $T^4 \approx 4T_a^3T - 3T_a^4$ (using Taylor series estimation), k* is the mean absorption coefficient, and $\sigma^*$is the Stefan-Boltzmann constant. Thus, we obtain

$$\frac{\partial q_r}{\partial r} \approx -\frac{16\sigma*T_a^3}{3k*}\frac{\partial^2 T}{\partial r^2}. \tag{8}$$

The dynamical temperature-dependent viscosity $\mu(T)$ is taken as

$$\mu(T) = \mu_0 e^{-m(T-T_a)}, \tag{9}$$

where μ_0 is the dynamic viscosity of the fluid at ambient temperature T_a so that $T_a < T_0$, m material property, z is the axial length, K is the porous medium's permeability, c is the Forchheimer inertial coefficient, r is the radial length, δ is the slip coefficient, T denotes the temperature of the fluid, u stands for axial velocity, r_1, r_2 are the inside and outside radii respectively, ρ is the density of the fluid, $k$is the thermal conductivity of the fluid, P is the fluid pressure, β represents the volumetric thermal enlargement coefficient, E_G is the volumetric entropy production (generation) rate, g represents acceleration as a result of gravity, h is the heat transfer coefficient. Using dimensionless variables

$$\bar{P} = \frac{\rho r_1^2 LP}{\mu_0^2},\ w = \frac{\rho u r_1}{\mu_0},\ \eta = \frac{r-r_1}{r_1 L}, Z = \frac{z}{r_1 L},\ \theta = \frac{T-T_a}{T_0-T_a},\ L = \frac{r_2-r_1}{r_1},$$

$$\gamma = m(T_0 - T_a),\ Gr = \frac{\rho g\beta r_1^3 L^2(T_0-T_a)}{\mu_0^2},\ Ns = \frac{E_g r_1^2 L^2}{k},\ Pr = \frac{\mu_0 c_p}{k},$$

$$Ec = \frac{\mu_0^2}{\rho^2 r_1^2 c_p(T_0-T_a)},\ \varepsilon = -\frac{\partial \bar{P}}{\partial Z},\ Bi = \frac{hr_1 L}{k},\ Nr = \frac{16\sigma^* T_a^3}{3kk^*},$$

$$Da = \frac{K}{r_1^2 L^2},\ \lambda = \frac{\mu_0}{\delta r_1 L},\ F = \frac{cL^2 r_1^2}{\sqrt{K}}, \tag{10}$$

the dimensionless controlling equations in addition to the suitable boundary conditions can be written as:

$$\frac{d^2w}{d\eta^2} - \gamma\frac{dw}{d\eta}\frac{d\theta}{d\eta} + \left(\frac{L}{L\eta+1}\right)\frac{dw}{d\eta} + (Gr\theta - Fw^2 + \varepsilon)e^{\gamma\theta} - \frac{w}{Da} = 0, \tag{11}$$

$$(1+Nr)\frac{d^2\theta}{d\eta^2}+\left(\frac{L}{L\eta+1}\right)\frac{d\theta}{d\eta}+PrEce^{-\gamma\theta}\left(\frac{dw}{d\eta}\right)^2+\frac{PrEc}{Da}e^{-\gamma\theta}w^2+FPrEcw^3=0, \quad (12)$$

$$Ns=(1+Nr)\left[\frac{d\theta}{d\eta}\right]^2+PrEce^{-\gamma\theta}\left(\frac{dw}{d\eta}\right)^2+\frac{PrEce^{-\gamma\theta}w^2}{Da}+FPrEcw^3, \quad (13)$$

with

$$w(0)=\lambda e^{-\gamma}\frac{dw}{d\eta}(0),\ \ \theta(0)=1,\ \ w(1)=0,\ \ \frac{d\theta}{d\eta}(1)=-Bi\theta(1), \quad (14)$$

where γ is the decrease rate of fluid viscosity due to temperature variation, *Nr* is the thermal radiation parameter, Da is the Darcy number, *F* is the Forchheimer inertial parameter, λ is the slip parameter, ε is the pressure gradient variable, Gr is the Grashof number, C_p represents the specific heat at a steady pressure, *L* denotes the concentric cylinder annulus parameter, Pr is the Prandtl variable, Ec refers to the Eckert number, Bi represents the thermal Biot number and η denotes the dimensionless annulus in the two cylinders. The other relevant parameters are skin friction (Cf) and Nusselt number (Nu), expressed as:

$$Cf=\frac{r_1L\tau}{\mu_0U}=e^{-\gamma\theta(\eta)}\frac{dw(\eta)}{d\eta}\Big|_{\eta=0,1},$$
$$Nu=\frac{r_1Lq}{k(T_0-T_a)}=-(1+Nr)\frac{d\theta(\eta)}{d\eta}\Big|_{\eta=0,1} \quad (15)$$

where $\tau=\mu(T)\frac{du}{dr}\Big|_{r_1,r_2}$, $q=-k\left(1+\frac{16\sigma^*T_a^3}{3kk^*}\right)\frac{dT}{dr}\Big|_{r_1r_2}$. The Bejan number (Be) is defined as

$$Be=\frac{N_1}{Ns}=\frac{N_1}{N_1+N_2}, \quad (16)$$

where $N_2=PrEce^{-\gamma\theta}\left(\frac{dw}{d\eta}\right)^2+\frac{PrEce^{-\gamma\theta}w^2}{Da}+FPrEcw^3$ is the entropy generation as a result of viscous dissipation and porous medium resistance heating, $N_1=(1+Nr)\left[\frac{d\theta}{d\eta}\right]^2$ represents the irreversibility owning to heat exchange.

3 Numerical Procedure

In the interest of solving the non-linear boundary value problem defined by Eqs. (11)-(14), the shooting approach combined with the Runge-Kutta-Fehlberg integration approach are numerically employed [21, 22]. Suppose that

$$w = y_1, w' = y_2, \theta = y_3, \theta' = y_4. \tag{17}$$

We modify the controlling equations into a set of non-linear initial value problems:

$$\left.\begin{aligned} y_1' &= y_2 \\ y_2' &= \gamma y_2 y_4 - \left(\frac{L}{L\eta+1}\right) y_2 + (Fy_1^2 - Gry_3 - \varepsilon) e^{\gamma y_3} + \frac{y_1}{Da} \\ y_3' &= y_4 \\ y_4' &= -\left(\frac{L}{L\eta+1}\right)\frac{y_4}{(1+Nr)} - \frac{PrEc}{(1+Nr)} e^{-\gamma\theta} y_2^2 - \frac{PrEc e^{-\gamma\theta}}{(1+Nr)Da} y_1^2 - \frac{FPrEc}{(1+Nr)} y_1^3 \end{aligned}\right\} \tag{18}$$

with the equivalent initial conditions given as:

$$y_1(0) = \lambda e^{-\gamma} y_2(0), y_2(0) = a_1, y_3(0) = 1, y_4(0) = a_2. \tag{19}$$

The unknown initial values of a_1 and a_2 in Eq. (19) are first assumed and thereafter determined precisely via the shooting procedure with an iteration technique using a Newton-Raphson step size of $\Delta\eta$ = 0.01. The solutions obtained numerically for the velocity and temperature contours are utilized to work out the values of skin friction, Nusselt number, entropy production rate, and Bejan number as stipulated in Eq. (15) together with Eq. (16).

4 Results and Discussion

The calculation results show the effects of the variation of the thermophysical parameters on fluid temperature, velocity, Nusselt number, skin friction, entropy generation rate, and Bejan number, as presented in Figures 2-7. The parameter value range employed in our numerical calculation (Gr = 1-2.5; Nr = 0.1-1.5; ε = 1-4; L = 0.5-3.5; etc.) was selected in order to give an insight into their impact on the overall thermal and flow structure within the annulus. In order to verify the precision of our numerical approach, we consider a special case of constant viscosity fluid flow within a no-slip concentric annulus without porous medium with L = 2, $Da = \infty$, ε = 1, Gr = F = λ = γ = 0, whose exact solution for the velocity profile in Eq. (11) is given as:

$$w(\eta) = -\frac{\varepsilon\eta}{4L}(L\eta + 2) + \frac{\varepsilon(L+2)}{4L}\frac{ln(L\eta+1)}{ln(L+1)}. \tag{20}$$

A comparison between the exact solution as obtained by Eq. (20) and the results obtained from the shooting method combined with the Runge-Kutta-Fehlberg integration are displayed in Table 1, showing excellent agreement. This confirms the precision of our numerical results.

Table 1 Computations exhibiting the correspondence between exact and numerical solution for L = 2, $Da = \infty$, $\varepsilon = 1$, $Gr = F = \lambda = \gamma = 0$.

η	$w(\eta)$ **Exact solution**	$w(\eta)$ **Shooting numerical solution**
0	0.000000000	0.0000000000
0.1	0.0554781164	0.0554781163
0.2	0.0931351142	0.0931351142
0.3	0.1164078699	0.1164078697
0.4	0.1275132396	0.1275132398
0.5	0.1279648767	0.1279648765
0.6	0.1188424088	0.1188424087
0.7	0.1009429931	0.1009429930
0.8	0.0748719992	0.0748719991
0.9	0.0410999908	0.0410999910
1.0	0.0000000000	0.0000000000

The effects of concentric gap parameter, pressure gradient, Grashof number, Forchheimer inertial parameter, and Darcy number on the velocity parameter are presented in Figure 2. It can be seen in Figure 2(a) that with an increase in the concentric gap parameter, the fluid velocity in the annular gap decreases. This may be attributed to the existence of wall shear stress, which has a great impact on the flow motion. It can be seen from Figure 2(b) that the pressure gradient was the main driving force. By increasing the pressure gradient, the velocity profile shoots up within the annulus gap.

The buoyancy effect on the flow was also examined through the Grashof number. A rise in the Grashof number automatically transfers to an increase in the temperature difference, which leads to a rise in the velocity profile, as can be seen in Figure 2(c). Moreover, an increase in temperature difference enhances the flow convection. The influence of the Darcy number on the velocity profile is displayed in Figure 2(d). An increase in the Darcy number causes an increase in the permeability of the porous medium. As a result, there exists little resistance in the flow through the porous medium. This causes the velocity to increase. Figure 2(e) presents the influence of the Forchheimer inertial parameter on the velocity profile. A decreasing effect is noticed at the center of the gap with an increase of the Forchheimer inertial parameter.

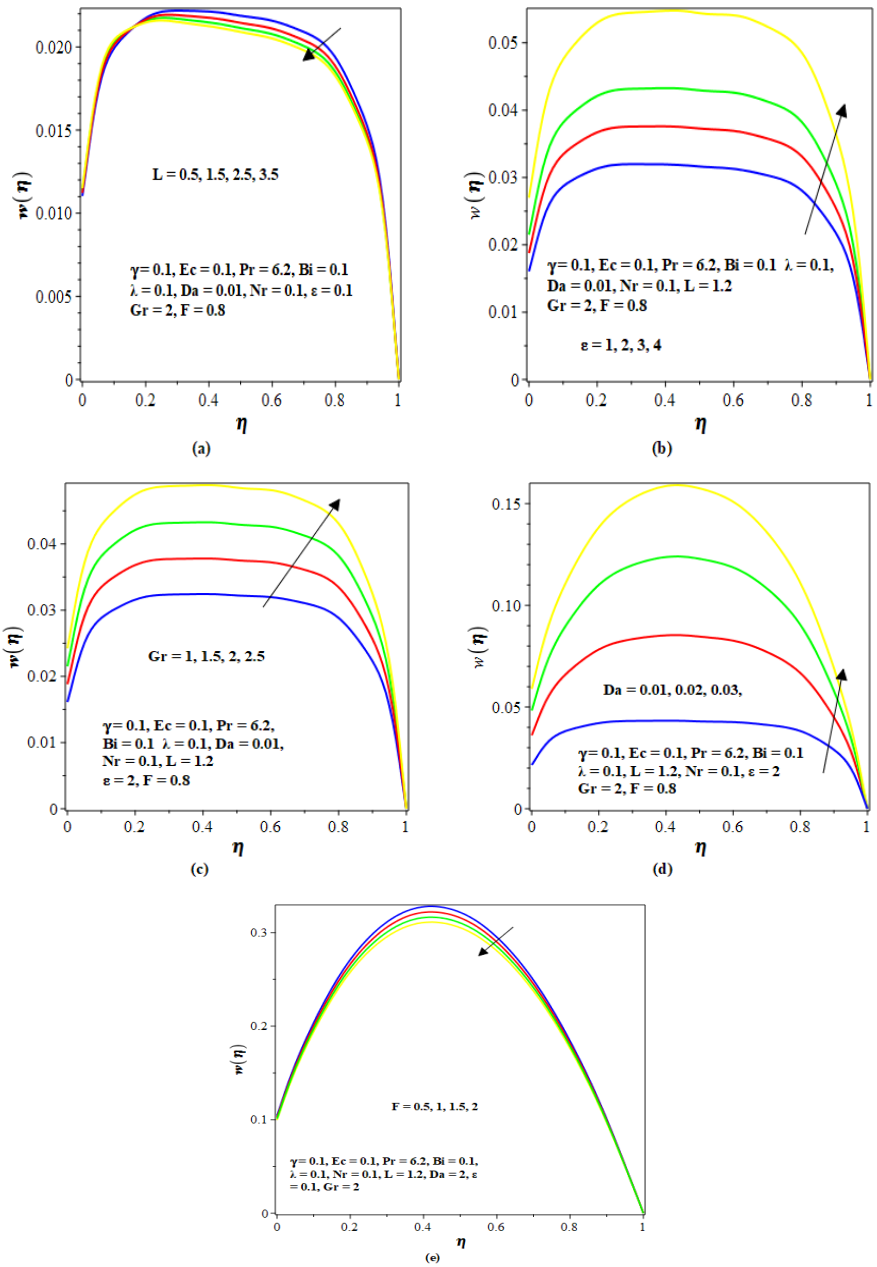

Figure 2 (a) Velocity profile with increasing L, (b) velocity profile with increasing ε, (c) velocity profile with increasing Gr, (d) velocity profile with increasing Da, (e) velocity profile with increasing F.

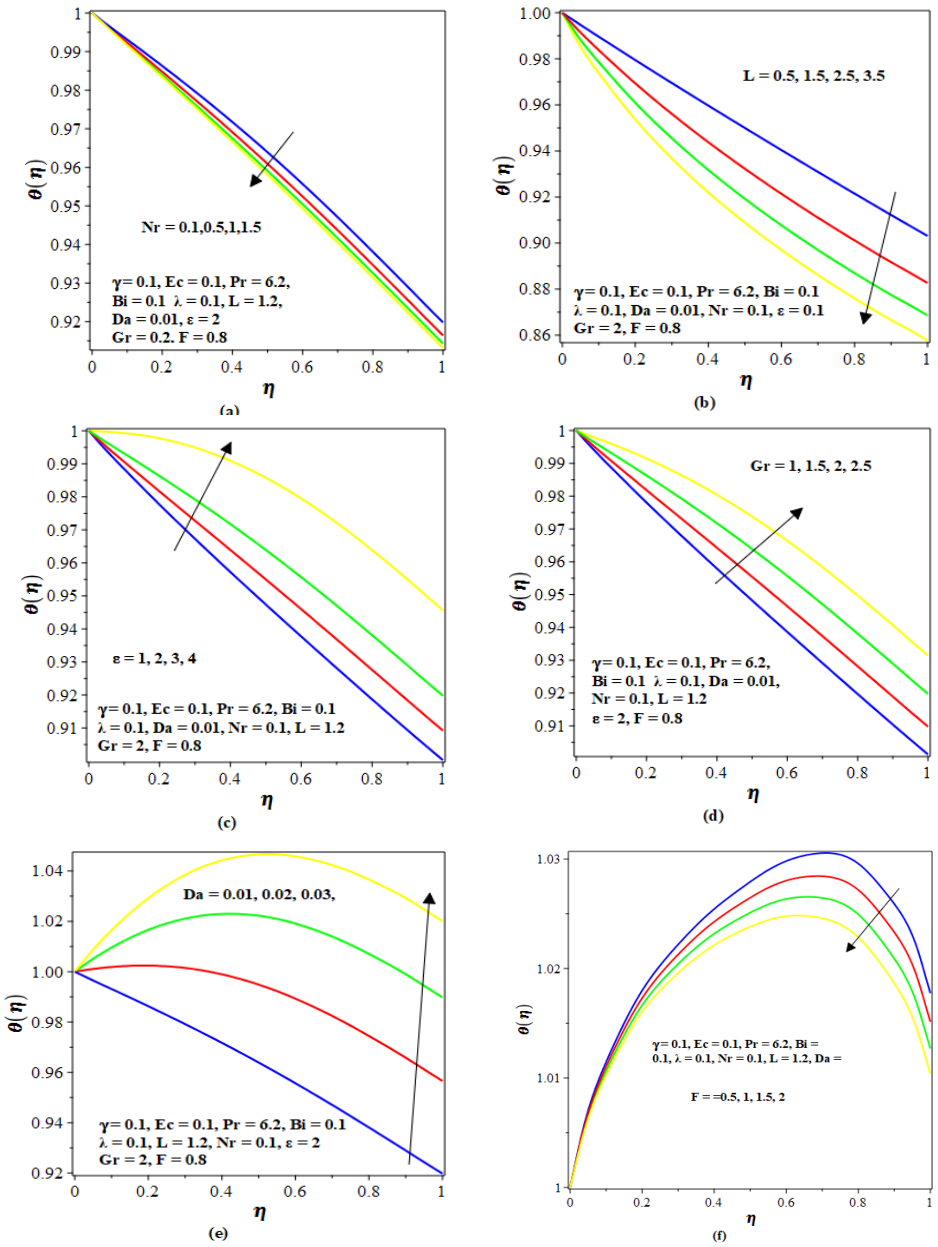

Figure 3 (a) Temperature profile with increasing Nr, (b) temperature profile with increasing L, (c) temperature profile with increasing ε, (d) temperature profile with increasing Gr, (e) temperature profile with increasing Da, (f) temperature profile with increasing F.

Figure 3 presents the effect of the thermal radiation parameter, concentric gap parameter, pressure gradient, Grashof number, Darcy number and Forchheimer inertial parameter on the temperature profile. The effect of the thermal radiation parameter on the temperature profile is presented in Figure 3(a). It can be seen that the temperature profile decreases with higher thermal radiation parameters because an increase in the thermal radiation parameter $\left(Nr = \frac{16\sigma^* T_a^3}{3kk^*}\right)$ for a given k and T_a leads to a decrease in mean absorption coefficient k^*. From Eqs. (3) and (7) we conclude that the local radiative heat flux term for optically thick gray fluid increases as the mean absorption coefficient decreases the rate of heat exchange to the fluid and thereby decreases the temperature profile.

The effect of the concentric gap parameter is shown in Figure 3(b). It is noted that as the concentric gap parameter goes up, the temperature profile decreases, which is more pronounced at the exterior of the pipe. Figure 3(c) shows the effect of the pressure gradient on the temperature profile. It can be seen that an increase in the pressure gradient causes the fluid molecules to increase and thereby raise the temperature contour. The effect of the Grashof number on the temperature profile is shown in Figure 3(d). The Grashof number correlates with the buoyancy and the viscous force acting on the fluid. The Grashof number and the boundary layer are proportional to each other; a rise in one leads to a rise in the other. It can be seen that increasing the Grashof number transfers more thermal energy to the fluid molecules and thereby relaxes the intermolecular forces in the fluid particles, which results in an increase of heat exchange in the fluid.

Figures 3(e)-(f) show the effects of the Darcy number and the Forchheimer inertial parameter on the temperature profile. It can be seen that any increase in the temperature profile at the outer pipe will increase the Darcy number while a decrease occurs in the temperature profile by increasing the Forchheimer inertial parameter, as shown in Figure 3(f).

The effects of pressure gradient versus thermal radiating parameter, Grashof number versus thermal radiating parameter, Darcy number versus thermal radiating parameter and Forchheimer inertial parameter versus thermal radiating parameter on both skin friction and Nusselt number are presented in Figures 4 and 5. In Figures 4 (a)-(c) it can be seen that as the pressure gradient versus the thermal radiating parameter, the Grashof number versus the thermal radiating parameter and the Darcy number versus the thermal radiating parameter are increasing, the skin friction also increases at both the interior and exterior of the pipes. However, the skin friction decreases as the Forchheimer inertial parameter versus the thermal radiating parameter increases, as shown in Figure 4(d).

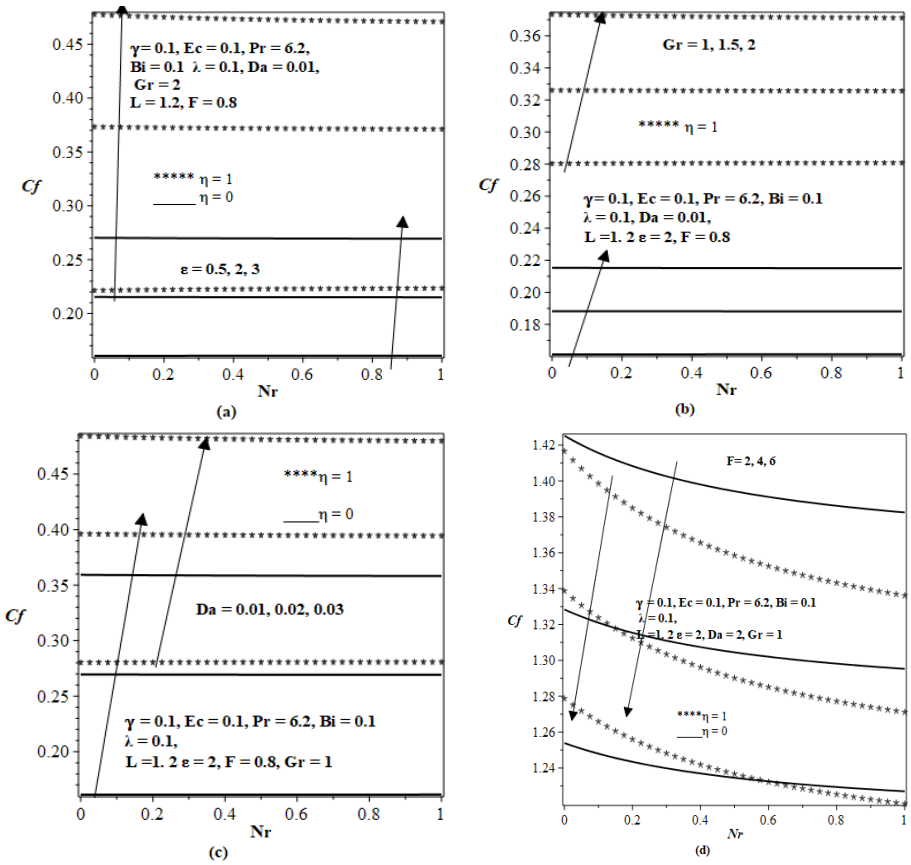

Figure 4 (a) Skin friction with increasing *Nr* and ε, (b) skin friction with increasing *Nr* and *Gr*, (c) skin friction with increasing *Nr* and *Da*, (d) skin friction with increasing *Nr* and *F*.

The significance of these parameters is also reflected in the Nusselt number shown in Figure 5. We observe that an increase in these variables leads to a reduction in the Nusselt number at both the interior and exterior of the pipes, as shown in Figures 5(b)-(d). However, the outer pipe in Figure 5(a) increases slightly with an increase in the concentric gap parameter versus the thermal radiating parameter.

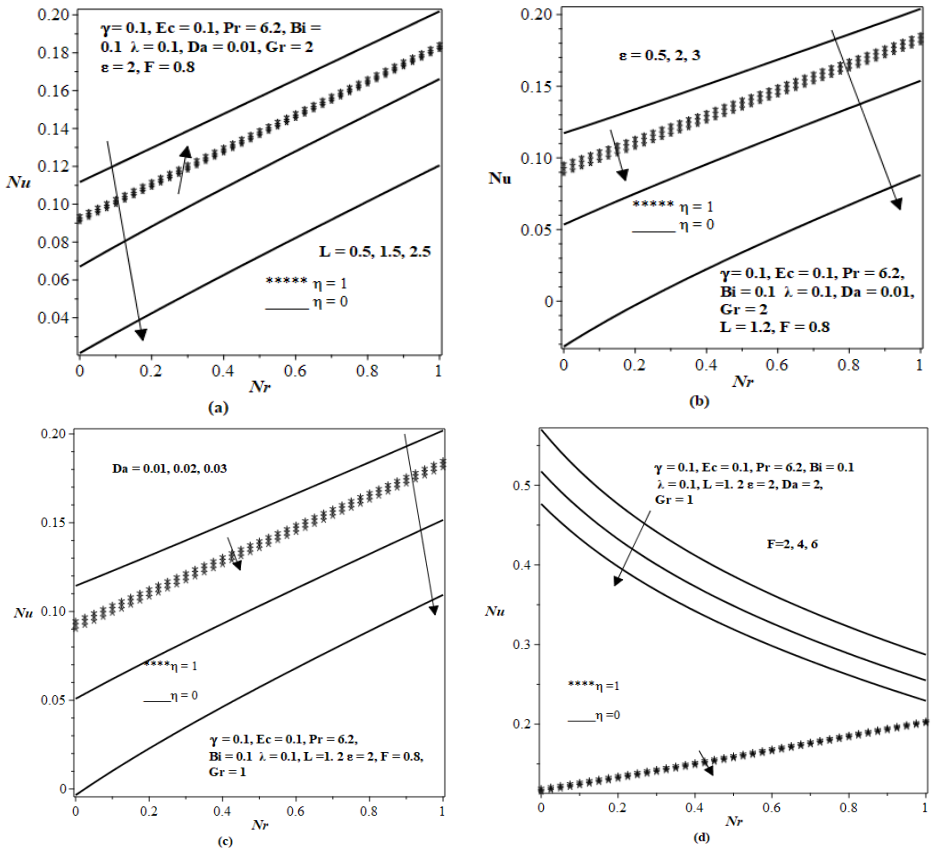

Figure 5 (a) Nusselt number with increasing *Nr* and *L*, (b) Nusselt number with increasing *Nr* and *ε*, (c) Nusselt number with increasing *Nr* and *Da*, (d) Nusselt number with increasing *Nr* and *F*.

Figure 6 present the effects of the thermal radiation parameter, concentric gap parameter, pressure gradient, Grashof number, Darcy number and Forchheimer inertial parameter on the entropy generation rate profile. In Figure 6(a), the entropy profile increases with increasing thermal radiating parameter in the flow channel and inside the pipes but with little effect on the outer pipe. It can be seen that there is a restrictive medium, which leads to a high disorder of the flow particles inside the pipe and increases the entropy generation, while little or no effect of the restrictive medium is detected at the outer pipe. Figure 6(b) details the influence of the concentric gap parameter on the entropy profile. Here, we see that the entropy profile increases at the inner wall and toward the channel center as the concentric gap parameter increases. Meanwhile, there is no effect from the middle of the gap to the outer pipe. We conclude from this

result that the restrictive medium gradually fades away from the inner pipe toward the outer pipe.

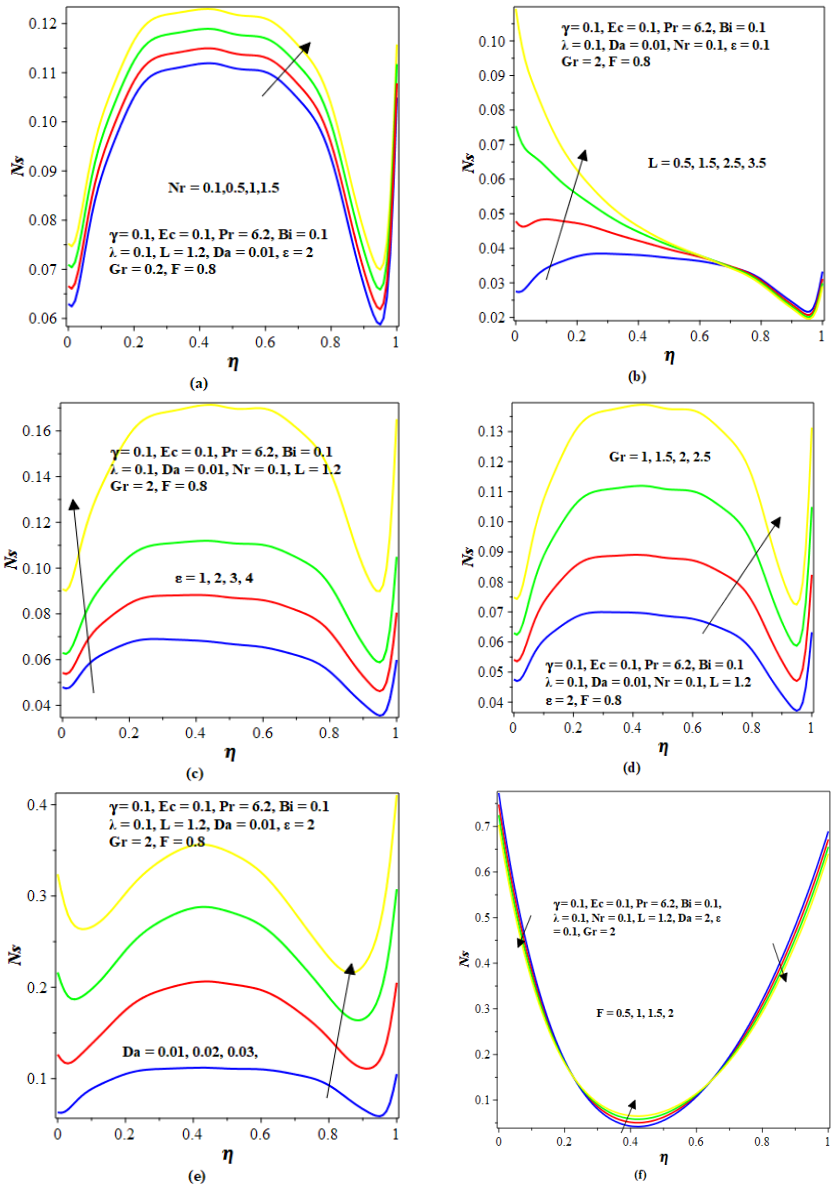

Figure 6 (a) Entropy profile with increasing Nr, (b) entropy profile with increasing L, (c) entropy profile with increasing ε, (d) entropy profile with increasing Gr, (e) entropy profile with increasing Da, (f) entropy profile with increasing F.

The effect of the pressure gradient on the entropy profile is revealed in Figure 6(c). It can be seen that an increase in the pressure gradient enhances the entropy profile throughout the flow channel and the same explanation applies to Figures 6(d)-(e), which show the effects of the Grashof number and the Darcy number. The effect of the Forchheimer inertial parameter is presented in Figure 6(f). We notice a slight decrease in the entropy generation rate in both pipes and a slight increase at the center of the gap as the Forchheimer inertial parameter increases.

The effect of varied values of the thermal radiation parameter, concentric gap parameter, pressure gradient, Grashof number, Darcy number and Forchheimer inertial parameter on the Bejan number profile are shown in Figure 7. In Figure 7(a) we see that an increase of the thermal radiating parameter increases the Bejan number profile within the flow channel. This implies that irreversibility due to heat exchange has a dominant effect on the flow. Figure 7(b) shows the effect of the concentric gap parameter on the Bejan number. This figure shows that the Bejan number increases inside the pipe with increasing concentric gap parameter while there is no impact of the Bejan number on the outer pipe. This shows that the dominant effect of the irreversibility resulting from heat transfer is more visible inside the pipe.

The influence of the pressure gradient on the Bejan number is illustrated in Figure 7(c). Here we see that the Bejan number decreases throughout the flow with an increase of the pressure gradient parameter. This implies that the entropy generation rate, as a result of viscous dissipation and porous medium resistance heating, has a dominant effect on the flow. With an increase of the Grashof number, as shown in Figure 7(d), the Bejan number decreases. The decrease in the Bejan number is more obvious at the inner pipe compared to the outer pipe. This shows that the dominant effect of entropy generation related to viscous dissipation and porous medium resistance heating is greater at the inner pipe compared to the outer pipe. The effect of variation of the Darcy number on the Bejan number is shown in Figure 7(e). It can be seen that the Darcy number increases the Bejan number at the inner wall while it reduces it at the outer wall of the pipe. Meanwhile, the Forchheimer inertial parameter reduces the Bejan number from the inner wall towards to center of the gap and slightly increases it from the same point towards the outer wall, as shown in Figure 7(f).

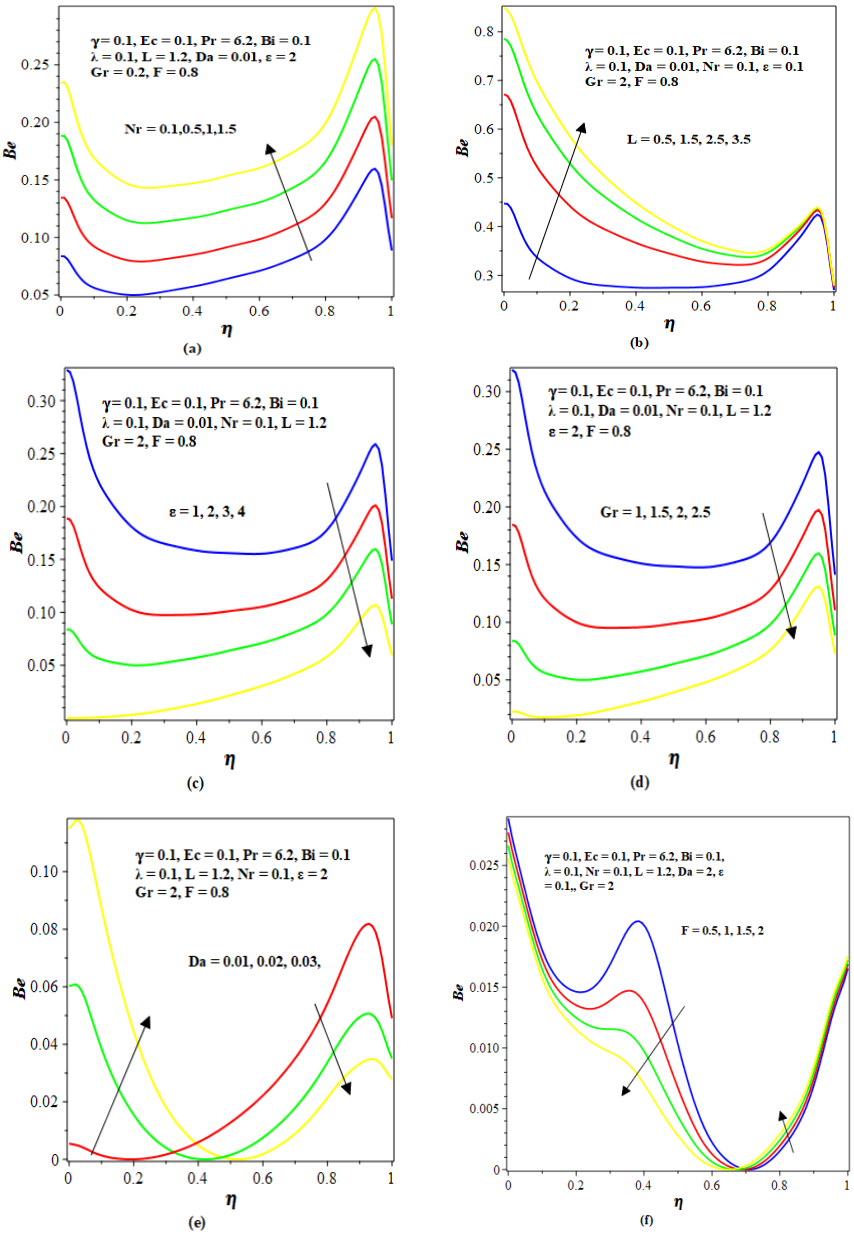

Figure 7 (a) Bejan number profile with increasing Nr, (b) Bejan number profile with increasing L, (c) Bejan number profile with increasing ε, (d) Bejan number profile with increasing Gr, (e) Bejan number profile with increasing Da, (f) Bejan number profile with increasing F.

5 Conclusions

The buoyancy convection of an inconstant viscosity radiating fluid within a slippery annulus formed between two concentric pipes filled with a porous medium was numerically examined via the shooting method coupled with the Runge-Kutta-Fehlberg integration method. Our results can be summarized as follows:

- Fluid velocity increases with increasing Grashof number, pressure gradient and Darcy number while it decreases with a rise in thermal radiation, annulus gap and Forchheimer inertial parameter.
- The fluid temperature increases with an increase in Grashof number, pressure gradient and Darcy number but decreases with an increase in thermal radiation, annulus gap and Forchheimer inertial parameter.
- The skin friction increases with increasing thermal radiation, annulus gap, Grashof number and Darcy number but decreases with increasing Forchheimer inertial parameter.
- The Nusselt number increases slightly with increasing thermal radiation parameter concentric gap parameter and decreases with increasing thermal radiation, annulus gap, Grashof number, Darcy number and Forchheimer inertial parameter in both vertical pipes.
- An increase of the Grashof number, pressure gradient, thermal radiation, annulus gap and the Darcy number leads to an increase of the entropy generation rate.
- An increase of the annulus gap boosts the Bejan number and increases the heat transfer irreversibility, while an increase in the Grashof number and pressure gradient decreases it. A rise in Darcy number increases the Bejan number at the inner wall, while the Forchheimer inertial parameter decreases the Bejan number at the inner wall.

Finally, it is noteworthy that suitable fine-tuning of the thermophysical parameters will enhance the entropy generation minimization in engineering thermal and fluid flow applications such as concentric pipe heat exchangers involving buoyant convection in a porous medium for optimal performance.

6 Nomenclatures

Be = Bejan number
Bi = Thermal Biot number
Cf = Skin friction
C_p = Specific heat at constant pressure $(J\text{Kg}/K)$
Da = Darcy number
Ec = Eckert number

E_G = Volumetric entropy generation
F = Forchheimer inertial parameter
Gr = Grashof number
g = Acceleration due to gravity (m/s^2)
h = Heat transfer coefficient (W/m^2k)
k = Fluid thermal conductivity $(Wm^{-1}K^{-1})$
m = Material property
N_1 = Irreversibility because of heat transfer
N_2 = Entropy generation because of viscous dissipation
Ns = Dimensionless entropy production rate
Nu = Nusselt number
Nr = Radiating parameter
P = Fluid pressure (N/m^2)
Pr = Prandtl number
r_1, r_2 = Inward and outward pipes radii (m)
r = Radial distance (m)
T = Fluid temperature $(°K)$
T_0 = Temperature at the inner pipe surface $(°K)$
T_a = Ambient temperature $(°K)$
u = Dimensional axial velocity (m/s^2)
w = Dimensionless axial velocity(m/s^2)
z = Axial distance

Greek Symbols

μ_0 = Fluid dynamic viscosity (the ambient temperature). (Ns/m^2)
μ = Dynamic viscosity of the fluid (Ns/m^2)
ρ = Density of the fluid (Kg/m^2)
β = Volumetric thermal expansion coefficient (K^{-1})
σ = Fluid electrical conductivity $(\Omega^{-1}m^{-1})$
γ = Decrease in fluid viscosity rate due to temperature difference
η = Dimensionless gap between two-cylinder
ε = Dimensionless axial pressure gradient
θ = Dimensionless temperature
λ = Slip parameter

References

[1] Watanabe, T., Toya, Y. & Nakamura, I., *Development of Free Surface Flow Between Concentric Cylinders with Vertical Axes*, Journal of Physics: Conference Series, **14**, pp. 9-19, 2005.

[2] Fénot, M., Bertin, Y., Dorignac, E. & Lalizel, G., *A Review of Heat Transfer Between Concentric Rotating Cylinders with or without Axial*

Flow, International Journal of Thermal Sciences, **50**, pp. 1138-1155, 2011.

[3] Makinde, O.D., *Thermal Analysis of a Reactive Generalized Couette Flow of Power-Law Fluid Between Concentric Cylindrical Pipes*, European Physical Journal Plus, **129**(270), 2014.

[4] Lorenzini, M., Dapra, I. & Scarpri, G., *Heat Transfer for a Giesekus Fluid in a Rotating Concentric Annulus*. Applied Thermal Engineering, **122**, pp. 118-125, 2017.

[5] Coelho, P.M. & Pinho, F. T., *A Generalized Brinkman Number for Non-Newtonian Duct Flows.* Journal of Non-Newtonian Fluid Mechanics, **156**(3), pp. 202-206, 2009.

[6] Bejan, A., *Second-Law Analysis in Heat Transfer and Thermal Design.* Advance in Heat Transfer, **15**, pp. 1-58, 1982.

[7] Eegunjobi, A.S. & Makinde, O.D., *Entropy Generation Analysis in Transient Variable Viscosity Couette Flow Between Two Concentric Pipes*, Journal of Thermal Science and Technology, **9**(2), pp. 1-11, 2014.

[8] Jain, S., Kumar, V. & Bohra, S., *Entropy Generation in Generalized Couette Flow Through Porous Medium with Different Thermal Boundary Conditions*, International Journal of Energy & Technology, **7**, pp. 40-48, 2015.

[9] Makinde, O.D., *Irreversibility Analysis for Gravity-Driven Non-Newtonian Liquid Film Along with an Inclined Isothermal Plate*, Physica Scripta, **74**, pp. 642-645, 2006.

[10] Saouli, S. & Aiboud-Saouli, S., *Second Law Analysis of The Laminar Falling Liquid Film Along with an Inclined Heated Plate*, Inter. Comm. Heat Mass Transfer, **31**, pp. 879-886, 2004.

[11] Yurusoy, M., Yilbas, B.S. & Pakdemirli, M., *Non-Newtonian Fluid Flow in Annular Pipes and Entropy Generation: Temperature-dependent Viscosity*, Sadhana, **31**(6), pp. 683-695, 2006.

[12] Monaledi, R.L. & Makinde, O.D., *Entropy Analysis of a Radiating Variable Viscosity EG/Ag Nanofluid Flow in Microchannels with Buoyancy Force and Convective Cooling*, Defect and Diffusion Forum, **387**, pp. 273-285, 2018.

[13] Chakraborty, S. & Ray, S., *Performance Optimisation of Laminar Fully Developed Flow Through Square Ducts with Rounded Corners.* International Journal of Thermal Sciences, **50**(12), pp. 2522-2535, 2011.

[14] Marzougui, S., Bouabid, M., Mebarek-Oudina, F., Abu-Hamdeh, N., Magherbi, M. & Ramesh K., *A Computational Analysis of Heat Transport Irreversibility Phenomenon in a Magnetized Porous Channel.* International Journal of Numerical Methods for Heat & Fluid Flow, **31**(7), pp. 2197-2222, 2021.

[15] Mebarek-Oudina, F., Fares, R., Aissa, A., Lewis, R. W. & Abu-Hamdeh N.H., *Entropy and Convection Effect on Magnetized Hybrid Nano-Liquid*

Flow Inside a Trapezoidal Cavity with The Zigzagged Wall. International Communications in Heat and Mass Transfer, **125**, 105279, 2021.

[16] Venkateswarlu, M., Lakshmi, D.V. & Makinde, O.D., *Thermodynamic Analysis of Hall Current and Soret Number Effect on Hydromagnetic Couette Flow in a Rotating System with a Convective Boundary Condition.* Heat Transfer Research, **51**(1), pp. 83-102, 2020.

[17] Nayak, M. K., Hakeem, A.K.A., Ganga, B., Khan, M.I., Waqas, M. & Makinde, O.D., *Entropy Optimized MHD 3D Nanomaterial of Non-Newtonian Fluid: A Combined Approach to a Good Absorber of Solar Energy and Intensification of Heat Transport.* Computer Methods and Programs in Biomedicine, **186**, 105131 pp. 1-15, 2020.

[18] Shaw, S., Dogonchi, A.S., Nayak, M.K. & Makinde, O.D., *Impact of Entropy Generation and Nonlinear Thermal Radiation on Darcy-Forchheimer Flow of $MnFe_2O_4$-Casson/Water Nanofluid Due to a Rotating Disk: Application to Brain Dynamics*. Arabian Journal for Science and Engineering, **45**(7), pp. 5471-5490, 2020.

[19] Brewster, M.A., *Thermal Radiative Transfer and Properties*. New York: John Wiley and Sons, 1992.

[20] Rosseland, S., *Theoretical Astrophysics*. Oxford University, New York, USA, 1936.

[21] Na, T.Y., *Computational Methods in Engineering Boundary Value Problem*, Academic Press, 1979.

[22] Cebeci, T. & Bradshaw, P., *Physical and Computational Aspects of Convective Heat Transfer*. New York, USA: Springer, 1988.